EDGE ARTICLE

Check for updates

Supramolecular assembly affording a ratiometric two-photon fluorescent nanoprobe for quantitative detection and bioimaging†

Peng Wang,[a] Cheng Zhang,[a] Hong-Wen Liu, [iD][a] Mengyi Xiong,[a] Sheng-Yan Yin,[a] Yue Yang,[a] Xiao-Xiao Hu,[ab] Xia Yin,*[a] Xiao-Bing Zhang [iD]*[a] and Weihong Tan [iD][a]

Fluorescence quantitative analyses for vital biomolecules are in great demand in biomedical science owing to their unique detection advantages with rapid, sensitive, non-damaging and specific identification. However, available fluorescence strategies for quantitative detection are usually hard to design and achieve. Inspired by supramolecular chemistry, a two-photon-excited fluorescent supramolecular nanoplatform (TPSNP) was designed for quantitative analysis with three parts: host molecules (β-CD polymers), a guest fluorophore of sensing probes (Np–Ad) and a guest internal reference (NpRh–Ad). In this strategy, the TPSNP possesses the merits of (i) improved water-solubility and biocompatibility; (ii) increased tissue penetration depth for bioimaging by two-photon excitation; (iii) quantitative and tunable assembly of functional guest molecules to obtain optimized detection conditions; (iv) a common approach to avoid the limitation of complicated design by adjustment of sensing probes; and (v) accurate quantitative analysis by virtue of reference molecules. As a proof-of-concept, we utilized the two-photon fluorescent probe NHS–Ad-based TPSNP-1 to realize accurate quantitative analysis of hydrogen sulfide (H₂S), with high sensitivity and good selectivity in live cells, deep tissues and *ex vivo*-dissected organs, suggesting that the TPSNP is an ideal quantitative indicator for clinical samples. What's more, TPSNP will pave the way for designing and preparing advanced supramolecular sensors for biosensing and biomedicine.

Introduction

Optical visualization of vital biomolecules including gasotransmitters, enzymes, and nucleic acids holds a particularly prominent position owing to its high sensitivity, rapid response, non-damaging detection and real-time imaging.[1–3] To date, as powerful tools, small molecular fluorescent probes have realized biosensing for various biomolecules, offering simplicity in operation and satisfactory performance.[4–7] However, it should be noted that very little optimization work has been carried out on quantitative analysis for monitoring biomolecules in living cells, deep tissues, and organs. Current small molecular fluorescent probes have generally failed to achieve this goal due to their intrinsic limitations, such as short excitation wavelengths, shallow tissue penetration depths, environmentally sensitive fluorescence-intensity-based read-out, poor water-solubility and undesirable biocompatibility. Among them, ratiometric fluorescent probes are regarded as an alternative strategy for quantitative detection with self-calibration ability.[8–11] Nevertheless, complicated energy transfer strategies and unmanageable ratiometric read-out signals delay the extensive and efficient quantitative analysis of ratiometric probes in biosamples. Therefore, there is an urgent need to design a fluorescent detection platform to realize efficient quantitative bioanalysis, but it is still a significant challenge.

Since the Nobel Prize was awarded to host–guest and supramolecular chemistry, the field of supramolecular chemistry has attracted much attention from scientists, and numerous supramolecular systems have been developed to investigate their bioapplications.[12–16] Utilizing host–guest self-assembled supramolecular polymers between macrocyclic molecules and functionalized guest molecules has already become a robust and flexible method to afford biosensing nanoprobes, which show tunable or stimuli-responsive physicochemical signals, prominent physiochemical shielding, improved water-solubility, and enhanced biocompatibility as well as avoiding the cumbersome synthesis provided by macrocyclic host molecules.[17–19] Inspired by supramolecular

aMolecular Science and Biomedicine Laboratory, State Key Laboratory of Chemo/Biosensing and Chemometrics, College of Chemistry and Chemical Engineering, Collaborative Innovation Center for Chemistry and Molecular Medicine, Hunan University, Changsha, Hunan 410082, China. E-mail: xbzhang@hnu.edu.cn

bMolecular Science and Biomedicine Laboratory, State Key Laboratory of Chemo/Biosensing and Chemometrics, College of Life Sciences, Hunan University, Changsha, Hunan 410082, China
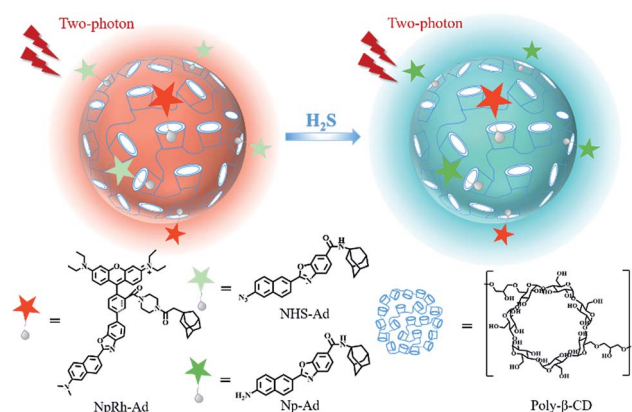
chemistry, we intend to build a fluorescent supramolecular quantitative analysis nanoplatform with three parts: host molecules, guest probe molecules and guest internal reference molecules.

Within the common supramolecular self-assembly systems, cyclodextrins (CDs) are a popular class of macrocyclic ring as host molecules by virtue of their ready availability from their starch precursors, functionalization of a variety of guests, satisfactory water solubility and low toxicity toward biological systems.[20–22] β-CD polymers (poly-β-CD) have been gradually used for molecular recognition, drug delivery and biosensing because of their large loading and tunable guest self-assembly.[23–26] Thus, poly-β-CD are the optimal choice for our nanoplatform strategy. To achieve deep tissue penetration, bioimaging with near-infrared (NIR) photons as the excitation source is expected. Two-photon microscopy (TPM), which excites a two-photon (TP) fluorophore with NIR laser pulses, has emerged as a novel and indispensable imaging tool for biosensing.[27–30] Compared with one-photon microscopy, TPM opens the opportunity for biosensing in living cells and deep tissues with the advantages of minimized fluorescence background, reduced photodamage, better three-dimensional spatial localization and increased penetration depth (>500 μm). Hence, based on our previous works, we chose a naphthalene-based TP fluorescent dye combined with adamantane (Np–Ad) as a fluorophore of the potential guest probes and TP through-bond energy transfer (TBET)-based rhodamine–adamantine (NpRh–Ad) as a TP guest internal reference with host nanoparticle poly-β-CD, to build a TP fluorescent supramolecular nanoplatform (TPSNP) for quantitative analysis. In this strategy, TPSNP would possess numerous merits from the host nanoparticles and functionalized guest molecules. First, poly-β-CD could improve the water-solubility and biocompatibility of small molecule fluorescent probes. Besides, as the host molecules, poly-β-CD could implement the quantitative and tunable assembly of functional guest molecules to obtain optimized conditions. Secondly, TP fluorescent guest molecules would increase the tissue penetration depth for bioimaging. Furthermore, this internal reference-doped supramolecular assembly strategy avoids the limitation of a complicated ratiometric design. Owing to the facile modification of Np–Ad, vast Np–Ad derivative probes could be utilized for various targets for physiological evaluation and disease diagnosis. To demonstrate the feasibility of the TPSNP design, hydrogen sulfide (H₂S) was chosen due to its essential role as a gasotransmitter in the human body as the model target for the TPSNP-1, which was assembled with the Np–Ad derivative H₂S sensing probe NHS–Ad, NpRh–Ad and poly-β-CD (Scheme 1).

Results and discussion

Preparation and characterization of the TPSNP

Poly-β-CD were synthesized according to previous literature.[31] ¹H NMR spectra showed that most of the bands of β-CD at 4.2–3.4 ppm were broadened in the spectrum of the poly-β-CD, which confirmed the successful synthesis of poly-β-CD (Fig. S1†). The morphology and size of the poly-β-CD were

Scheme 1 Schematic representation of the TPSNP-1 for H₂S quantitative detection.

investigated. Field emission scanning electron microscope (SEM) images showed that the poly-β-CD were spherical in shape and the size distribution was about 90 nm (Fig. S2†).

TBET is a flexible strategy to design ratiometric probes without the need for spectral overlap between the donor emission and the acceptor absorption.[32–35] Our group previously proposed a TBET system (Np–Rh), with a naphthalene derivative and rhodamine spirolactam to achieve deep-tissue imaging for Cu²⁺.[36] We introduced adamantine, a common guest molecule for β-CD, into the rhodamine portion of Np–Rh by amide linkage with piperazine (termed NpRh–Ad) to make rhodamine always keep its ring-opening form and emit red fluorescence. Meanwhile, we utilized the naphthalene-based TP fluorescent probe with green fluorescence to functionalize the poly-β-CD. Owing to the TBET strategy, two emission bands from the naphthalene-based fluorophore and the rhodamine moiety displayed weak interplay when the sensing probe was activated. NpRh–Ad, Np–Ad and NHS–Ad were efficiently synthesized by following the synthetic route shown in Scheme S1† and all of the reaction products were fully characterized by ¹H NMR, ¹³C NMR and mass spectrometry (see ESI, Fig. S16–S32†).

As a proof-of-concept, the poly-β-CD were incubated with NpRh–Ad (10 μM) and Np–Ad (5 μM) in a 10 mM phosphate buffered solution (PBS, pH = 7.4) at the same time and subjected to vibration treatment for 4 h at 300 rpm (25 °C). The morphology and size of the TPSNP were investigated using SEM, atomic force microscopy (AFM) and dynamic light scattering (DLS). The SEM and AFM images show that the self-assembled
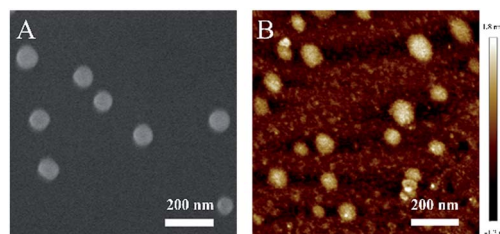

Fig. 1   (A) SEM and (B) AFM images of the TPSNP.

supramolecular nanoparticles were spherical in shape with a size distribution of ∼90 nm (Fig. 1), and its average hydrodynamic diameter in PBS was ∼140 nm by DLS analysis (Fig. S3†). There was no obvious change in the morphology and size between the **TPSNP** and poly-β-CD from the SEM images. To confirm the combination of the NpRh–Ad and/or Np–Ad with the poly-β-CD by supramolecular self-assembly, agarose gel electrophoresis (AGE) experiments were carried out. As can be seen in Fig. S4b,† under the effect of an electric field, NpRh–Ad and/or Np–Ad in the presence of poly-β-CD (channel 2, 4 and 5) remained owing to the high-molecular-weight, while the free dyes (channel 1 and 3) migrated. Furthermore, compared with the free NpRh–Ad and Np–Ad, the fluorescence emissions of NpRh–Ad/poly-β-CD and Np–Ad/poly-β-CD were both dramatically enhanced with 365 nm UV illumination (Fig. S4a†), which indicates the formation of NpRh–Ad/poly-β-CD and Np–Ad/poly-β-CD to improve the solubility of the corresponding dyes in buffer solution. These results are consistent with the previous literature that direct macrocyclic dye molecule host–guest supramolecular self-assembly enhanced the fluorescence intensity in aqueous solution.[37–39] Obviously, supramolecular polymers have an advantage for detection over our previously proposed probe, Np–Rh, in biosamples, which requires 10% ethyl alcohol in buffer solution to work rather than an absolute water solution.

Spectroscopic studies of the TPSNP *in vitro*

The spectroscopic properties of the **TPSNP** were studied in PBS (pH = 7.4). It should be pointed out that, compared with the single dye-doped **TPSNP**, the two dye-doped **TPSNP** showed satisfactory overlay of the absorption spectra and distinction of the fluorescence emission spectra (Fig. S5†). What's more, the red fluorescence region maintained no obvious difference after co-assembling (Fig. S5b†), suggesting that NpRh–Ad should be a competent TP internal reference. As shown in Fig. S6,† $1/(F − F_0)$ vs. $1/[\beta\text{-CD}]$ was a linear relationship, indicating the formation of a 1 : 1 host–guest supramolecular polymer between the dyes with β-CD. Analyzed by the Benesi–Hildebrand plot, the binding constant (K) of NpRh–Ad with poly-β-CD in PBS (pH = 7.4) was 2.5×10^2 M^{-1}, and that of Np–Ad with poly-β-CD was 2.5×10^3 M^{-1}. At the same time, more than 96% of the dyes combined with β-CD cavities of the poly-β-CD. To achieve the capability of imaging deep inside a tissue and at a higher spacial resolution, the TP active absorption cross-section of host–guest supramolecular polymer was investigated. As shown in Fig. 2, the TP active absorption cross-section of NpRh–Ad with the poly-β-CD was 118.55 GM (1 GM = 10^{-50} $(cm^4 s)$ per photon) at 780 nm, and that of Np–Ad with the poly-β-CD was 106.38 GM. According to our previous reports, the TP properties of the supramolecular polymer were similar to those of the free dyes, which certifies that the assembled nanoprobes keep the TP properties of dyes. We also studied the effect of pH on the **TPSNP** and Np–Ad/poly-β-CD. Compared with Np–Ad/poly-β-CD (Fig. S7b†), pH changes (from 3.0 to 13.0) had no obvious effect on the performance of the **TPSNP** (Fig. S7a†), indicating that the fluorescent internal reference system can
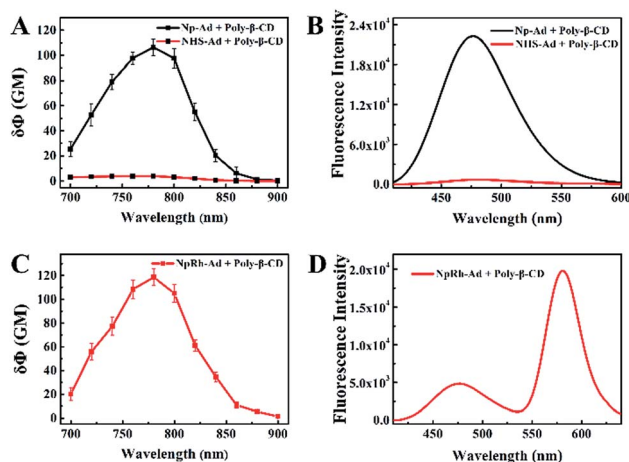

Fig. 2 (A) The TP active absorption cross-section and (B) TP excited emission spectra of Np–Ad (5 μM) and NHS–Ad (5 μM) with poly-β-CD in PBS (pH = 7.4). (C) The TP absorption cross-section and (D) TP excited emission spectra of NpRh–Ad (10 μM) with poly-β-CD in PBS (pH = 7.4); the excitation wavelength was 780 nm.

avoid interferences from the surroundings (such as pH value, viscosity and polarity) and have a predictable performance in its self-calibration ability. The stability of the **TPSNP** in the PBS (pH = 7.4) and cell culture medium was investigated by monitoring its fluorescence ratio (F_{475}/F_{575}) changes (Fig. S8†). The results showed that the prepared host–guest supramolecular polymer had good stability in detecting conditions and complex environments for long periods of time.

Cytotoxicity and intracellular uptake of the TPSNP

To elucidate its further bioapplication, the cytotoxicity of the **TPSNP** was first tested by MTS assays. As shown in Fig. S9,† the cells maintained high viability after incubation with the **TPSNP** for 24 h even at high concentrations, clearly indicating the low cytotoxicity of the **TPSNP** and suggesting its suitable application in intracellular sensing. To demonstrate the cellular uptake of this nanoprobe, imaging of HeLa cells was carried out after incubation with the **TPSNP** for different periods of time. As shown in Fig. S10,† the **TPSNP** were well internalized after 2 h of incubation. These results are consistent with vesicular uptake mechanisms for nanoparticles. The intracellular distribution of the **TPSNP** was also investigated by co-localization with a commercial lysosome-specific fluorescent dye, LysoTracker Red (Fig. S11†). The red fluorescence from the LysoTracker Red and the green fluorescence from the Np–Ad/poly-β-CD overlapped well with a Pearson's correlation factor of 0.9295, which indicated that the nanoprobe was localized in the lysosomes. Therefore, we speculated that the **TPSNP** could be internalized by cells and used for biosensing.

H2S sensing of the TPSNP-1 *in vitro*

To exhibit the outstanding performance of quantitative determination of biomolecules in living cells and deep tissues by using **TPSNP**, H2S was chosen as the model target for further

study. As an important member of the gasotransmitter family, H_2S has been identified in mediating many physiological systems, such as the central nervous system, immune system, and blood circulation system.[40–44] It is generally accepted that abnormal H_2S level in live cells would result in a variety of human diseases, such as Alzheimer's disease and Down's syndrome.[45,46] Therefore, it is of scientific interest to develop effective methods for the quantitative analysis of H_2S in biosystems. We previously proposed a naphthalene derivative-based TP fluorescent probe, termed NHS1, which could be used for rapid detection of endogenous H_2S in live cells.[47] Based on this research, we designed a TP fluorescent probe, NHS–Ad, and combined it with NpRh–Ad and poly-β-CD to construct a TP fluorescent supramolecular nanoprobe (TPSNP-1) for H_2S detection. TPSNP-1 operated through reaction between the H_2S and azide group of NHS–Ad, leading to reduction of the azide to an amino and fluorescence enhancement of the NHS–Ad.

The fluorescence spectra changes of the TPSNP-1 upon the gradual addition of H_2S were investigated. As shown in Fig. 3A, the addition of NaHS triggered a large fluorescence enhancement of the TPSNP-1 at 475 nm due to the production of Np–Ad. Furthermore, accompanying the fluorescence enhancement at 475 nm, the fluorescence intensity at 575 nm remain unchanged, which proved the outstanding performance of the TP internal reference. To verify the advantage of poly-β-CD in the quantitative and tunable assembly of guests, different molar ratios of NHS–Ad and NpRh–Ad were combined with the poly-β-CD for H_2S sensing. As shown in Fig. 3A and S12,† the ratios of the two dopants ranging from 4 : 1 to 1 : 2 made the H_2S-responsive sensitivity of the TPSNP-1 different. To obtain the optimal sensitivity and effectiveness of the internal reference,

we chose TPSNP-1 prepared with a molar ratio of 2 : 1 (NHS–Ad to NpRh–Ad) for further study. As can be seen from Fig. 3C, the F_{475}/F_{575} was linearly proportional to NaHS in the concentration range of 0–5 μM. The detection limit (S/N = 3) for NaHS was calculated to be 86 nM, which is favorable for direct imaging of intracellular H_2S, the concentrations of which are usually in a submicromolar range. Notably, the detection sensitivity of this nanoprobe is similar to that of the reported probe NHS1, which certifies that the predominant biosensing capacity of the small molecule probe is kept after being combined with the host–guest supramolecular system. The selectivity of the TPSNP-1 for H_2S was also investigated. As shown in Fig. S13,† the F_{475}/F_{575} of the TPSNP-1 exhibited no obvious changes in the presence of these potential intracellular coexisting species, which demonstrates the excellent selectivity of the TPSNP-1 for H_2S. The time-dependent fluorescence response was investigated. As shown in Fig. S14,† the fluorescence signal reached a plateau after about 40 min. The TP properties of NHS–Ad/poly-β-CD were investigated. As shown in Fig. 2A, the TP active absorption cross-section of NHS–Ad with poly-β-CD was 3.85 GM at 780 nm. The TP excited fluorescence spectra of the TPSNP-1 upon addition of H_2S are shown in Fig. 3D. A distinct TP excited fluorescence enhancement at 475 nm was observed upon excitation by 780 nm femtosecond pulses. The drastic TP excited fluorescence enhancement is favorable for intracellular H_2S imaging with high resolution and sensitivity by TPM.
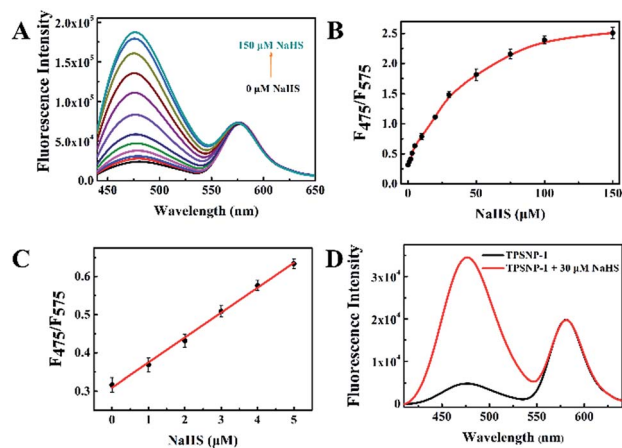

Fig. 3 (A) The fluorescence response of the TPSNP-1 (10 μM NHS–Ad + 5 μM NpRh–Ad + 10 mM Poly-β-CD) to NaHS at different concentrations (0, 1, 2, 3, 5, 10, 20, 30, 50, 75, 100 and 150 μM). (B) The calibration curve of the TPSNP-1 to NaHS. The curve was plotted with the fluorescence intensity vs. the NaHS concentration after incubation for 40 min. (C) The linear responses at low NaHS concentrations, $R = 0.997$. The standard curve of the TPSNP-1 response to H_2S is $y = 0.30947 + 0.06531x$. $\lambda_{ex} = 420$ nm. (D) The TP excited fluorescence response of the TPSNP-1 to NaHS (30 μM) in PBS (pH = 7.4); the excitation wavelength was 780 nm.
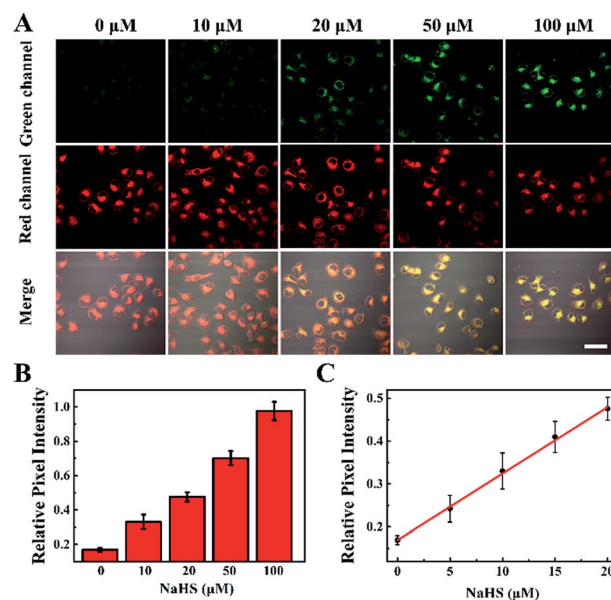

Fig. 4 (A) TP excited confocal fluorescence imaging of the TPSNP-1 in HeLa cells from the green channel and red channel with varied concentrations of NaHS (from left to right: 0, 10, 20, 50 and 100 μM). $\lambda_{ex} = 780$ nm; green channel, $\lambda_{em} = 440-540$ nm; red channel, $\lambda_{em} = 560-660$ nm. Scale bar: 40 μm. (B) The relative pixel fluorescence intensity of the ratio between the green channel and red channel. (C) Linear fitting curve of the relative pixel fluorescence intensity toward the low concentration of NaHS. The standard curve of the TPSNP-1 response to H_2S in HeLa cells is $y = 0.16918 + 0.0155x$ ($R = 0.999$).
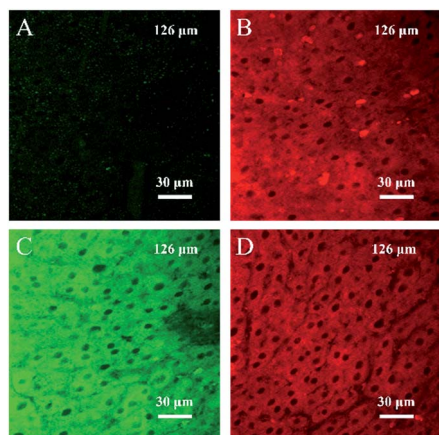
Fig. 5 TPM images of a fresh rat liver slice stained with the **TPSNP-1** at a depth of 126 μm with a magnification of 60×. Images were acquired using 780 nm excitation and fluorescent emission windows: (A and B) The **TPSNP-1** incubated without NaHS; (C and D) the **TPSNP-1** incubated with NaHS (100 μM); (A and C) green = 440–540 nm; (B and D) red = 560–660 nm. Scale bars: 30 μm.
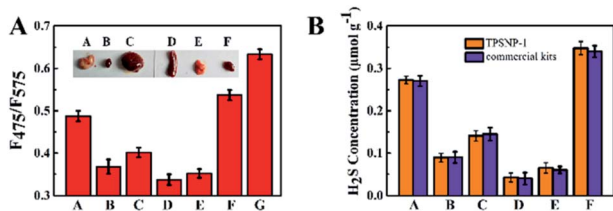

Fig. 6 Quantitative evaluation of H_2S concentration in *ex vivo*-dissected organs. (a) Brain, (b) heart, (c) liver, (d) spleen, (e) lung, (f) kidney and (g) NaHS (5 μM). (A) The fluorescence response of the **TPSNP-1** in the tissue homogenates. $\lambda_{ex} = 420$ nm (B) The comparison between the **TPSNP-1** and endogenous H_2S commercial kits for detection in the tissue homogenates. The values presented are normalized.

TP fluorescence imaging of H_2S in living cells and deep tissues

Owing to the highly sensitive and selective response to H_2S and its remarkable TP properties, TP excited confocal fluorescence imaging experiments of the **TPSNP-1** for H_2S in living HeLa cells were then carried out. As shown in Fig. 4A, incubation of the HeLa cells with the **TPSNP-1** afforded a gradually enhanced green fluorescence emission and steady red fluorescence emission when co-incubated with additional NaHS upon excitation at 780 nm. Notably, due to the presence of a red fluorescent internal reference, the green fluorescence emission enhancement could veritably reflect the response between the **TPSNP-1** and H_2S, avoiding the interference of fluorescence intensity from the surroundings, such as pH value, viscosity and polarity. Therefore, we could calculate the relative pixel fluorescence intensity of the HeLa cells images (Fig. 4B) and obtain a standard curve of the H_2S response (Fig. 4C).

To further show the excellent performance of the **TPSNP-1**, TP imaging of H_2S in rat normal liver tissue slices was carried out. The changes in fluorescence signal intensity with scan depth were recorded by TPM in the Z-scan mode. As can be seen from Fig. S15,† the **TPSNP-1** was capable of tissue imaging at depths of 80–170 μm by TPM. In the absence of exogenous H_2S, the green channel exhibited a weak TP fluorescence signal (Fig. 5A and S15A†), while the red channel had an intense signal (Fig. 5B and S15B†), indicating that the **TPSNP-1** had excellent tissue penetration and staining capabilities as well as non-interfering two-color (green and red) imaging ability. In addition, endogenic H_2S in the normal rat liver tissue was at a low level. When NaHS was added, a drastic TP fluorescence signal enhancement was observed in the green channel (Fig. 5C and S15C†) and the fluorescence signal intensity of the red channel almost remained the same (Fig. 5D and S15D†). These data showed that the **TPSNP-1** not only achieved TP fluorescence imaging in deep tissues but also possessed the power of ratiometric TP imaging by virtue of the red fluorescent TP internal reference.

H_2S quantitative analysis in organs by the TPSNP-1

Since the **TPSNP-1** demonstrated excellent performance in cells and deep tissues, we attempted to quantitatively evaluate the concentrations of H_2S in *ex vivo*-dissected organs. As can be seen from the inset of Fig. 6, we dissected the living mice to get the visceral organs, including the brain, heart, liver, spleen, lung and kidney. Then fluorescence tests with the **TPSNP-1** and commercial kits for endogenous H_2S were carried out. We calculated the content of H_2S in the aforementioned organs on the basis of the standard curve of the **TPSNP-1**, and made a comparison with that of H_2S commercial kits (Fig. 6). The results demonstrated that the **TPSNP-1** had a remarkable property for quantitative analysis of physiological factors. As shown in Fig. 6, the concentrations of H_2S in the brain and kidney were much higher than that in the other organs. It is well known that H_2S is a neuromodulator and neuroprotectant in the brain, and a wide range of H_2S concentrations are reported from undetectable to micromolar, which are determined by brain activity.[48] The fact that endogenous H_2S related enzyme cystathionine γ-lyase (CSE) is at a high level may lead to a higher concentration of H_2S in the kidney.[49] Hence, the **TPSNP-1** offered exciting opportunities for quantitative analysis in various organs and was promising for clinical samples to diagnose disease.

Conclusions

In summary, we developed a novel two-photon-excited supramolecular nanoplatform **TPSNP** based on the host–guest supramolecular recognition between the TP fluorophore of a potential guest probe (Np–Ad), a TP guest internal reference (NpRh–Ad) and host nanoparticles (poly-β-CD). The **TPSNP** exhibited outstanding physicochemical properties (supramolecular self-assembly, spectroscopic properties, TP property and stability), feasible cell uptake and good biocompatibility. Thanks to facile modification of Np–Ad, the **TPSNP** has the most significant potential in quantitative analysis for biomolecules for physiological evaluation and disease diagnosis. We

employed the **TPSNP-1** to realize the quantitative analysis of gasotransmitter H_2S in living cells, deep tissues and *ex vivo*-dissected organs with satisfactory performance (high sensitivity, good selectivity, deep tissue imaging and accurate quantitative detection). What's more, the **TPSNP** is conducive to widening the functions and applications of supramolecular chemistry. We believe that the TP fluorescent supramolecular nanoplatform, **TPSNP**, will pave the way for designing and preparing advanced supramolecular sensor materials for biosensing and biomedicine.

Conflicts of interest

There are no conflicts to declare.

Acknowledgements

Notes and references

1 X. Li, X. Gao, W. Shi and H. Ma, *Chem. Rev.*, 2014, **114**, 590–659.

2 J. A. Thomas, *Chem. Soc. Rev.*, 2015, **44**, 4494–4500.

3 W. Xu, Z. Zeng, J. H. Jiang, Y. T. Chang and L. Yuan, *Angew. Chem., Int. Ed.*, 2016, **55**, 13658–13699.

4 A. R. Lippert, E. J. New and C. J. Chang, *J. Am. Chem. Soc.*, 2011, **133**, 10078–10080.

5 Y. Gabe, Y. Urano, K. Kikuchi, H. Kojima and T. Nagano, *J. Am. Chem. Soc.*, 2004, **126**, 3357–3367.

6 D. Asanuma, M. Sakabe, M. Kamiya, K. Yamamoto, J. Hiratake, M. Ogawa, N. Kosaka, P. L. Choyke, T. Nagano, H. Kobayashi and Y. Urano, *Nat. Commun.*, 2015, **6**, 6463.

7 X. Wu, L. Li, W. Shi, Q. Gong and H. Ma, *Angew. Chem., Int. Ed.*, 2016, **55**, 14728–14732.

8 J. Fan, M. Hu, P. Zhan and X. Peng, *Chem. Soc. Rev.*, 2013, **42**, 29–43.

9 K. Gu, Y. Liu, Z. Guo, C. Lian, C. Yan, P. Shi, H. Tian and W. H. Zhu, *ACS Appl. Mater. Interfaces*, 2016, 26622–26629.

10 Z. Dai, L. Tian, B. Song, Z. Ye, X. Liu and J. Yuan, *Anal. Chem.*, 2014, **86**, 11883–11889.

11 C. Huang, T. Jia, M. Tang, Q. Yin, W. Zhu, C. Zhang, Y. Yang, N. Jia, Y. Xu and X. Qian, *J. Am. Chem. Soc.*, 2014, **136**, 14237–14244.

12 B. Shi, K. Jie, Y. Zhou, J. Zhou, D. Xia and F. Huang, *J. Am. Chem. Soc.*, 2016, **138**, 80–83.

13 P. Xing and Y. Zhao, *Adv. Mater.*, 2016, **28**, 7304–7339.

14 Y. Zhou, W. Huang, J. Liu, X. Zhu and D. Yan, *Adv. Mater.*, 2010, **22**, 4567–4590.

15 R. Dong, Y. Zhou, X. Huang, X. Zhu, Y. Lu and J. Shen, *Adv. Mater.*, 2015, **27**, 498–526.

16 J. Murray, K. Kim, T. Ogoshi, W. Yao and B. C. Gibb, *Chem. Soc. Rev.*, 2017, **46**, 2479–2496.

17 X. Ma and Y. Zhao, *Chem. Rev.*, 2015, **115**, 7794–7839.

18 G. Yu, K. Jie and F. Huang, *Chem. Rev.*, 2015, **115**, 7240–7303.

19 J. Hu and S. Liu, *Acc. Chem. Res.*, 2014, **47**, 2084–2095.

20 S. Li and W. C. Purdy, *Chem. Rev.*, 1992, **92**, 1457–1470.

21 T. Irie and K. Uekama, *J. Pharm. Sci.*, 1997, **86**, 147–162.

22 M. E. Brewster and T. Loftsson, *Adv. Drug Delivery Rev.*, 2007, **59**, 645–666.

23 R. Liu, Y. Zhang and P. Feng, *J. Am. Chem. Soc.*, 2009, **131**, 15128–15129.

24 L. He, X. Yang, F. Zhao, K. Wang, Q. Wang, J. Liu, J. Huang, W. Li and M. Yang, *Anal. Chem.*, 2015, **87**, 2459–2465.

25 H. Yan, L. He, C. Ma, J. Li, J. Yang, R. Yang and W. Tan, *Chem. Commun.*, 2014, **50**, 8398–8401.

26 H. Yan, L. He, W. Zhao, J. Li, Y. Xiao, R. Yang and W. Tan, *Anal. Chem.*, 2014, **86**, 11440–11450.

27 H. M. Kim and B. R. Cho, *Chem. Rev.*, 2015, **115**, 5014–5055.

28 G. S. He, L.-S. Tan, Q. Zheng and P. N. Prasad, *Chem. Rev.*, 2008, **108**, 1245–1330.

29 H. M. Kim and B. R. Cho, *Acc. Chem. Res.*, 2009, **42**, 863–872.

30 H. W. Liu, Y. Liu, P. Wang and X. B. Zhang, *Methods Appl. Fluoresc.*, 2017, **5**, 012003.

31 C. Koopmans and H. Ritter, *Macromolecules*, 2008, **41**, 7418–7422.

32 G. S. Jiao, L. H. Thoresen and K. Burgess, *J. Am. Chem. Soc.*, 2003, **125**, 14668–14669.

33 W. Lin, L. Yuan, Z. Cao, Y. Feng and J. Song, *Angew. Chem., Int. Ed.*, 2010, **49**, 375–379.

34 J. Fan, P. Zhan, M. Hu, W. Sun, J. Tang, J. Wang, S. Sun, F. Song and X. Peng, *Org. Lett.*, 2013, **15**, 492–495.

35 H. W. Liu, X. B. Zhang, J. Zhang, Q. Q. Wang, X. X. Hu, P. Wang and W. Tan, *Anal. Chem.*, 2015, **87**, 8896–8903.

36 L. Zhou, X. Zhang, Q. Wang, Y. Lv, G. Mao, A. Luo, Y. Wu, Y. Wu, J. Zhang and W. Tan, *J. Am. Chem. Soc.*, 2014, **136**, 9838–9841.

37 F. Biedermann, E. Elmalem, I. Ghosh, W. M. Nau and O. A. Scherman, *Angew. Chem., Int. Ed.*, 2012, **51**, 7739–7743.

38 H. J. Kim, D. R. Whang, J. Gierschner and S. Y. Park, *Angew. Chem., Int. Ed.*, 2016, **55**, 15915–15919.

39 R. N. Dsouza, U. Pischel and W. M. Nau, *Chem. Rev.*, 2011, **111**, 7941–7980.

40 L. Li, P. Rose and P. K. Moore, *Annu. Rev. Pharmacol. Toxicol.*, 2011, **51**, 169–187.

41 J. M. Fukuto, S. J. Carrington, D. J. Tantillo, J. G. Harrison, L. J. Ignarro, B. A. Freeman, A. Chen and D. A. Wink, *Chem. Res. Toxicol.*, 2012, **25**, 769–793.

42 R. Wang, *Physiol. Rev.*, 2012, **92**, 791–896.

43 P. K. Yadav, M. Martinov, V. Vitvitsky, J. Seravalli, R. Wedmann, M. R. Filipovic and R. Banerjee, *J. Am. Chem. Soc.*, 2016, **138**, 289–299.

44 K. Ono, T. Akaike, T. Sawa, Y. Kumagai, D. A. Wink, D. J. Tantillo, A. J. Hobbs, P. Nagy, M. Xian, J. Lin and J. M. Fukuto, *Free Radical Biol. Med.*, 2014, **77**, 82–94.

45 K. Eto, T. Asada, K. Arima, T. Makifuchi and H. Kimura, *Biochem. Biophys. Res. Commun.*, 2002, **293**, 1485–1488.

46 M. Lee, C. Schwab, S. Yu, E. McGeer and P. L. McGeer, *Neurobiol. Aging*, 2009, **30**, 1523–1534.

47 G. J. Mao, T. T. Wei, X. X. Wang, S. Y. Huan, D. Q. Lu, J. Zhang, X. B. Zhang, W. Tan, G. L. Shen and R. Q. Yu, *Anal. Chem.*, 2013, **85**, 7875–7881.

48 Y. Qian, L. Zhang, S. Ding, X. Deng, C. He, X. E. Zheng, H.-L. Zhu and J. Zhao, *Chem. Sci.*, 2012, **3**, 2920–2923.

49 C. A. Wagner, *J. Nephrol.*, 2009, **22**, 173–176.